IOP Conf. Series: Materials Science and Engineering **322** (2018) 042004 doi:10.1088/1757-899X/322/4/042004

A Peridynamic Approach for Nanoscratch Simulation of the Cement Mortar

Jingjing Zhao[1], Qing Zhang [2], Guangda Lu [3], Depeng Chen [1]

[1]Department of Engineering Management, Anhui university of technology Ma Anshan, 243000, PR China
[2]Department of Engineering Mechanics, Hohai University, Nanjing, 210098, PR China
[3]Department of civil engineering ,Tongji University, Shanghai, 200092, PR China

Abstract. The present study develops a peridynamic approach for simulating the nanoscratch procedure on the cement mortar interface. In this approach, the cement and sand are considered as discrete particles with certain mechanical properties on the nanoscale. Besides, the interaction force functions for different components in the interface are represented by combining the van der Waals force and the peridynamic force. The nanoscratch procedures with the indenter moving along certain direction either parallel or perpendicular to the interface are simulated in this paper. The simulation results show the damage evolution processes and the final damage distributions of the cement mortar under different scratching speed and depth of the indenter, indicating that the interface between cement and sand is a weak area.

1. Introduction

The main research purpose on the ITZ is to explore whether or not the ITZ has influences on the mechanical properties of cement-based materials [1]. For this problem, there are two opposite opinions. Some people think that it is the weakest area, so that it plays an important role by influencing the properties of cement-based materials[2-4]. However, other researchers pointed out that there is no direct evidence to prove that when the concrete with the water cement ratio of 0.5, ITZ will cause significant negative effects on the mechanical properties of concrete [5]. Although many experiments about ITZ have been carried out, due to the inappropriate experimental method itself, there is still no conclusive evidence to support either one of the aforementioned opinions[6].

With the development of experimental technique, scanning electron microscope, mercury intrusion method, X-ray method, back scattered electron imaging and nanoindentation, nanoscratch and other techniques have been used to characterize the microstructure mechanical properties of ITZ. Throughout those researches, it is generally believed that the mechanical properties of concrete which influenced by ITZ is mainly focused on the strength, fracture mechanics and elastic modulus.

C-S-H accounts for 50-70% in hydration products of cement paste. At the same time, it contributes to the macroscopic properties such as the durability and cohesion of concrete the most[7,8]. According to Jennings and Tennis model, there are two forms of C-S-H in the cement paste, low-density C-S-H and high-density C-S-H[9]. Based on this model and experimental carried out by Allen, the numerical model of C-S-H can be supposed with a collection of 5 nm diameter particles as a gel material [10-11]. In this paper, cement paste is assumed to be spherical particles of high-density C-S-H. In addition, the sand is also regarded as dispersed particles of 5 nm in diameter. The packing fraction for the cement paste and sand phase is assumed to be 74%. And, according to the packing density, the numerical

model adopts the hexagonal close packing (HCP) structure. Combining the van der Waals force and peridynamic force, the force functions of different components in the interface of cement mortar are proposed in this simulation. The nanoscratch simulations are performed along with different scratching direction. One is the indenter scratching parallel to the interface. And the other is the indenter scratching perpendicular to the interface. The results show the damage evolution and damage distribution of the model under different scratching speed and depth. At the same time, the results could also point that the interface between cement and sand is a weak area.

2. Simulation method and process

A new theory, called the peridynamics（PD）method which was proposed by Silling several years ago suppose a force between two particles with a certain range. PD theory uses the integral formulation instead of the spatial partial differentia equations in classical continuum mechanics. Therefore, a crack with a discontinuity surface can be effectively solved by the PD theory.And the PD method provides a natural way to combine the van der Waals force and peridynamic force[12]。 In order to analyze the influence of ITZ on the nanoscale mechanical properties of concrete, the nanoscratch simulations are performed with different scratching direction. Combining the van der Waals force and peridynamic force, the force functions of different components in the interface of cement mortar are proposed. In this paper, the simulation process using FORTRAN language program.

2.1. Particle forces functions

2.1.1. The force between the cement paste. The force function between the cement paste has three parts: long-range van der Waals forces, cohesive forces of short-range electrostatic surface charge and peridynamic force.

When $0 < y < 1.1d$， the PD constitutive function proposed by Silling is used as follows[13]:

$$f_1 = cs \tag{1}$$

Where $\boldsymbol{\xi} = \boldsymbol{x}' - \boldsymbol{x}$ and $\boldsymbol{\eta} = \boldsymbol{u}' - \boldsymbol{u}$, which are the relative position and relative displacement, respectively. $y = |\boldsymbol{\xi} + \boldsymbol{\eta}|$ is the relative distance after deformation. The constant micro-modulus c can be written as

$$\mathrm{c} = \frac{18\mathrm{K}}{\pi\delta^4} \tag{2}$$

Where K is the bulk modulus, expressed as:

$$K = \frac{E}{3\times(1-2\nu)} \tag{3}$$

in which E is the elastic modulus of the material and the Poisson's ratio $\nu = 0.25$. The particle diameter is $d = 5nm$ [14]. The parameter δ called horizon size is set to be $3d = 15nm$.And the stretch s is defined as

$$s(t,\eta,\xi) = \frac{\|\eta+\xi\| - \|\xi\|}{\|\xi\|} \tag{4}$$

Where the relative position $\boldsymbol{\xi} = \boldsymbol{x}' - \boldsymbol{x}$ and the relative displacement $\boldsymbol{\eta} = \boldsymbol{u}' - \boldsymbol{u}$. And $s < s_0(t,\eta,\xi)$, here s_0 is A critical stretch .When $s \geq s_0$, f_1 is set to be zero.

When $d < y < 1.02d$, the short-range cohesive force is as follows:

$$f_2 = -1.5nN \tag{5}$$

Here f_2 is an adjustable parameter. Many researchers pointed out that the values of f_2 determined to be approximately 1 nN [15,16].

When $1.1d > y \geq 1.02d$, the long-range van der Waals forces are assumed to be the primary force between particles[17]. which can be defined by:

$$f_3 = -\frac{A}{6d}\left[\frac{2(a+1)}{a^2+2a} - \frac{a+1}{(a^2+2a)^2} - \frac{2}{a+1} - \frac{1}{(a+1)^3}\right] \tag{6}$$

Where $a = (y-d)/d$ and the Hamaker's constant $A = 10^{-20} J$. And the value of Hamaker's constant falls between the values for mica and amorphous silica [18].
When $y \geq 1.1d$,

$$f_4 = 0 \tag{7}$$

2.1.2 The force between the sand and the force between the sand and cement. Because there is no cohesion between the sand, so there is no need to add the short-range electrostatic force and long-range van der Waals force. Therefore, this paper assumes that the force between the sand is only PD force. At the same time, the interaction force between sand and cement also ignores the cohesion, therefore the force function between the cement and sand can have the same form. The PD constitutive function proposed by Silling is as follows:

$$f = \mu c(\boldsymbol{\xi}, \delta) s \tag{8}$$

Where constant c is shown in Eq.(2) and μ is a scalar-valued function defined by

$$\mu(t, \boldsymbol{\eta}, \boldsymbol{\xi}) = \begin{cases} 1, & s(t', \boldsymbol{\eta}, \boldsymbol{\xi}) < \min\left(s_0(t', \boldsymbol{\eta}, \boldsymbol{\xi}), s_0(t', \boldsymbol{\eta}', \boldsymbol{\xi}')\right) \\ & 0 \leq t' \leq t \\ 0, & otherwise \end{cases} \tag{9}$$

Where the stretch s and critical stretch s_0 are shown in Eq.(4).

2.2 Cement mortar with damage
In order to describe the local damage degree of material point, by using statistical methods, the damage D is defined as follows[19]:

$$D(x) = 1 - \frac{\int_H \mu(x, \xi) dV'}{\int_H dV'} \tag{10}$$

Where μ is a scalar-valued function and also is a discontinuous function to characterize whether the bond between two material points is broken, when the fracture occurs, the value is 0, whereas the opposite is 1. The value range of $D(x)$ is $0 \leq D \leq 1$, As shown in Figure 1, the value of D=0 indicates that there is no damage and indicating that the material is in the elastic deformation stage, and the value of $D \approx 0.5$, indicates that half of the bonds between the material points have been broken.

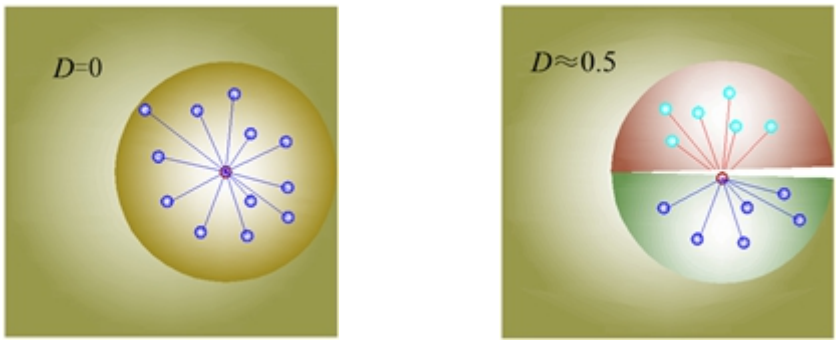

(a) When $D = 0$ (b) when $D \approx 0.5$

Figure 1. The damage for material point

2.3 Model establishment

In the simulations, a conical indenter with a 15-nm radius and high 30mm scratch a box with dimensions of $100 \times 100 \times 60 nm^3$. The nanoscratch simulations are performed with different scratching direction. One is the indenter scratching parallel to the interface. and the other is the indenter scratching perpendicular to the interface. The nanoscratch depth used in the simulations is 5nm. Spherical particles were placed according to a hexagonal close packing (HCP) arrangement with packing density 0.74[14]. The models can be divided into two parts, as shown in Figure 2. The green area represents sand and the red area represents cement paste. The diameter of all spherical particles is 5nm. In addition, the cement paste particle density was 2.6 g / cm^3 [20]and the sand particle density was 1.4 g / cm^3 . The chosen time step was 0.01ps. In this study, for cement paste a value of $E_a = 70GPa$ was adopted and for sand a value of $E_b = 110GPa$ was adopted[21]. Meanwhile, the simulation adopts an average elastic modulus $E_a = 90GPa$ for the interface of the sand and cement paste. A critical stretch s_0 is set to be 10^{-2}. The velocity-verlet algorithm was used and the relevant formula is as follows[22]:

$$\begin{cases} 1. & \mathbf{v}_i^{n+\frac{1}{2}} = \mathbf{v}_i^n + \dfrac{\Delta t}{2\rho_i}\tilde{\mathbf{f}}_i^n \\ 2. & \mathbf{y}_i^{n+1} = \mathbf{y}_i^n + \Delta t \mathbf{v}_i^{n+\frac{1}{2}} \\ 3. & \mathbf{v}_i^{n+1} = \mathbf{v}_i^{n+\frac{1}{2}} + \dfrac{\Delta t}{2\rho_i}\tilde{\mathbf{f}}_i^{n+1} \end{cases} \tag{11}$$

3. Results and analysis

3.1 Indenter scratching parallel to the interface

In the simulations, a conical indenter with a 15-nm radius and high 30mm scratching a box with a speed of $2000 nm / s$. The nanoscratch depth is 5nm. Figure 2 shows the morphology of the state of the model during the scratching process. The green area represents sand and the red area represents cement paste.

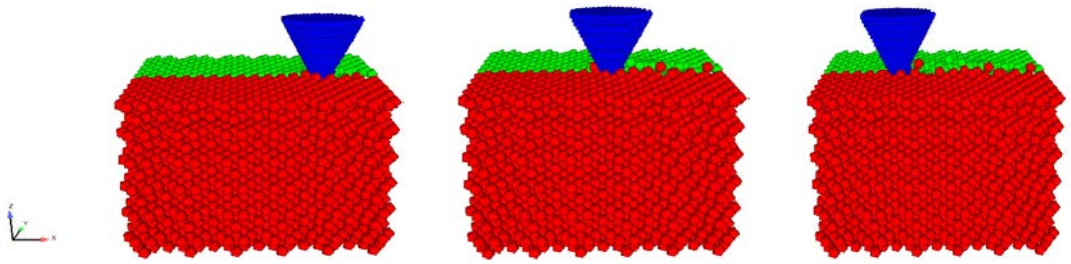

Figure 2. The model of indenter scratching parallel to the interface

It can be seen from the Figure 2, when the conical indenter moving forward constantly at the interface, the interface part which contacts with indenter has been deformation. Some particles in front of the indenter or on both sides of the indenter are raised and stacked. And a groove is carved. The particles are stacked on both sides of the groove to form a side flow. Figure 3 shows the damage distribution, when scratch distance is 70nm corresponding to the cutting speed of $1000nm/s$, $2000nm/s$, $4000nm/s$ respectively. Cement mortar in the Negative direction of Y axis, and the sand in the positive direction of Y axis.

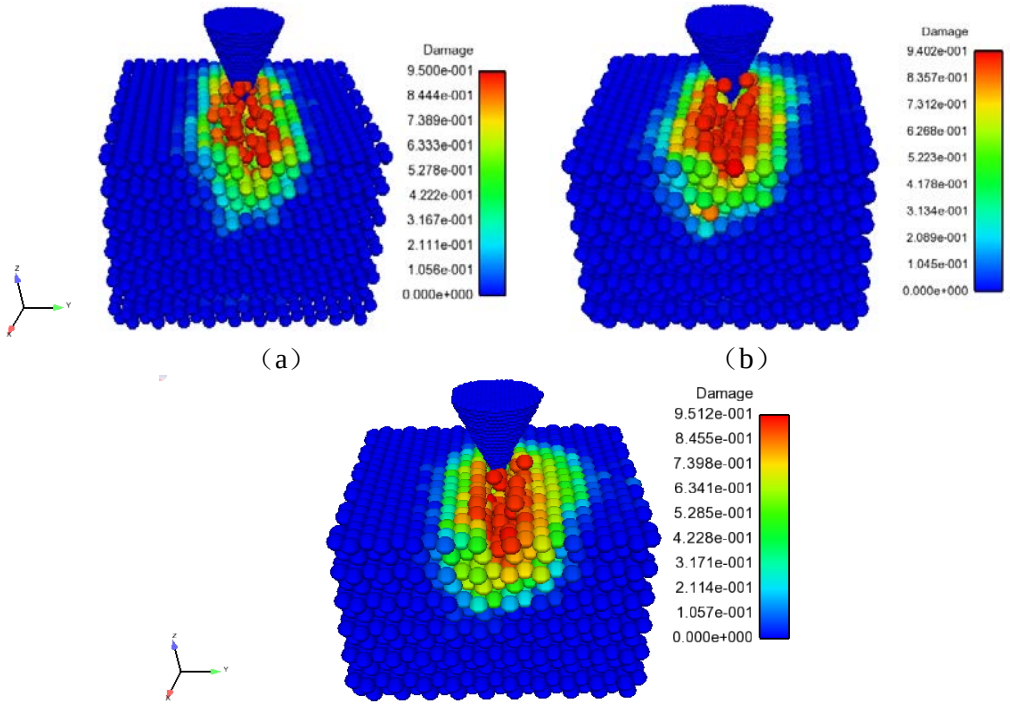

Figure 3. Graph of the damage versus the 70nm scratch distance for the scratching speed $1000nm/s$, $2000nm/s$, $4000nm/s$ respectively

It can be seen from the Figure 3, when the scratching distance is 70nm, the speed is respectively $1000nm/s$、$2000nm/s$、$4000nm/s$, and the interface part which contacts with indenter is almost completely damaged. Some particles scattered in both sides of the indenter, the other particles are at the bottom of the groove. Comparison both sides of the indenter, it can be found that with the speed increasing, the damage range of sand significantly increased. But the damage range of cement paste slightly changed. This phenomenon can also be seen from the profile at the interface (Figure 4).

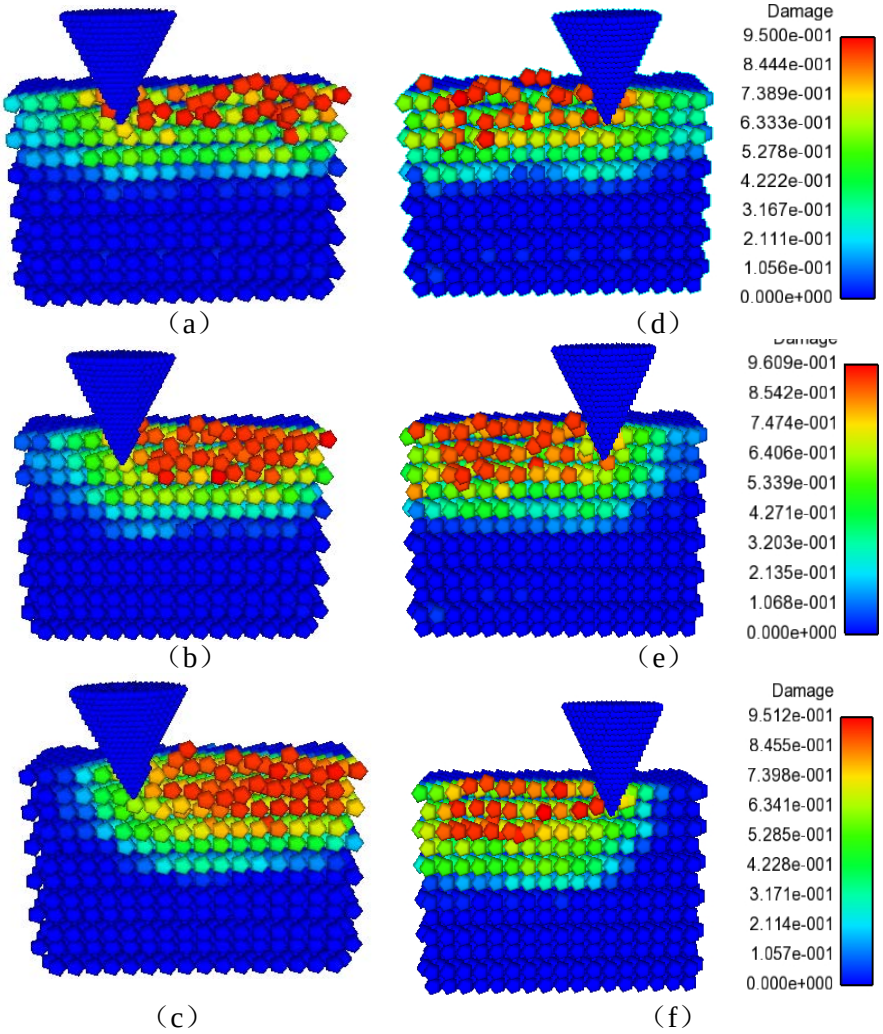

Figure 4. Graph of the damage versus the 70nm scratch distance for the scratching speed $1000nm/s$ (a,d), $2000nm/s$ (b,e), $4000nm/s$ (c,f)respectively. Graph a, b, c represent the damage profile of sand, Graph d, e, f represent the damage profile of cement paste.

Figure 4 shows the damage range of cement paste and sand at the interface, when the scratching distance is 70nm with different scratching speed. With the increasing of the speed, the severely damaged particles are gradually increased at the interface. The damage range is also expanding. Comparison the profile of cement paste and sand, it can be found that when the speed increases from $1000nm/s$ to $2000nm/s$, the severely damaged area of the cement paste and sand increase obviously. However, when the speed increases from $2000nm/s$ to $4000nm/s$, the damaged area of sand increases gradually. But the damaged area of cement paste has not change significantly. The main reason for this phenomenon is the cohesive force in the cementitious material.

Considering the influence of different scratching depth on interfacial damage, the scratching speed is set to be $2000nm/s$, to simulate the cutting process of $5nm, 10nm, 15nm$ depth respectively. Figure 4 shows the damage range of cement paste and sand at the interface, when the scratching distance is 70nm for different scratching depths.

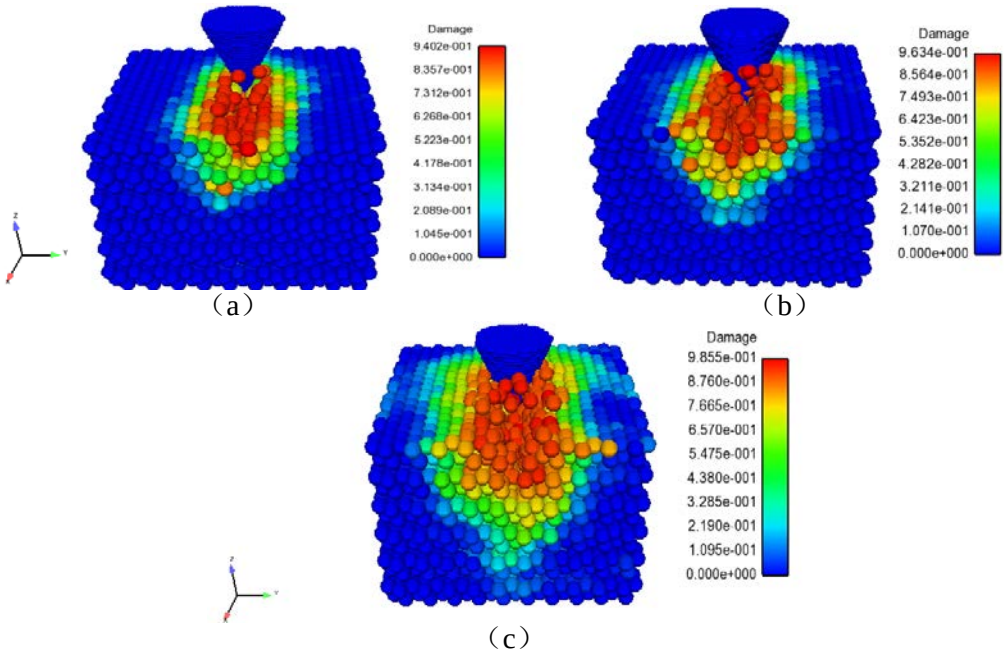

Figure 5. Graph of the damage versus the 70nm scratch distance for the scratching depth 5nm、10nm、15nm respectively.

It can be seen from the Figure 5, when the scratch distance is 70nm, with the increase of the scratch depth, the system deformation also increases, and the severely damaged area increases obviously as well. Especially when the scratching depth is 15nm, the damage degree and range of cement paste and sand along the interface are basically the same, morphology tends to symmetrical distribution.

3.2 Indenter scratching perpendicular to the interface

In the simulations, a conical indenter with a 15-nm radius and high 30mm scratching a box with a speed of $1000nm/s$. The nanoscratch depth is 5nm. Figure 6 shows the model morphology of the state of the scratching process. in which the green area represents sand and the red area represents cement paste.

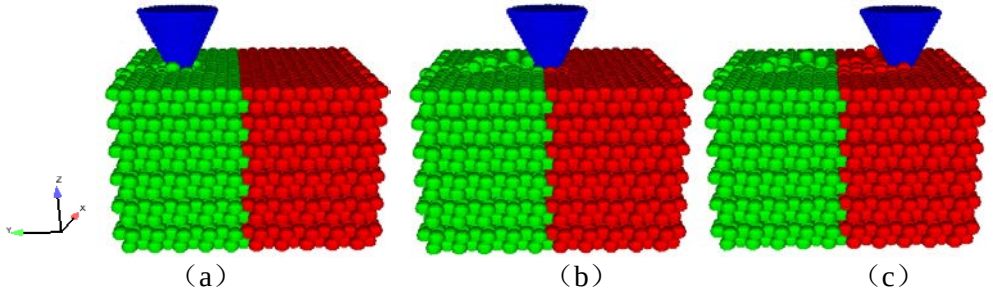

Figure 6. The model of indenter scratching perpendicular to the interface

Figure 6 shows the particles state of nanoscatching process.It can be seen from the figure, when the conical indenter moving forward constantly perpendicular to the interface, the part which contacts with indenter will deform. Some particles in front of the indenter or on both sides of the indenter are raised and stacked. And a groove is carved. The particles are stacked on both sides of the groove to form a side flow. Subsequently, the conical indenter moving forward to the cement paste portion, also some particles in front of the indenter or on both sides of the indenter are raised and stacked. And a groove is carved.

Considering the influence of different scratching speed on the interface, when the cutting depth is 5nm, supposing the scratching speed of $1000nm/s$, $2000nm/s$, $4000nm/s$ respectively. The

indenter scratches perpendicular to the interface from the end of the sand to the end of the cement paste, where the line is the interface (Figure 7).

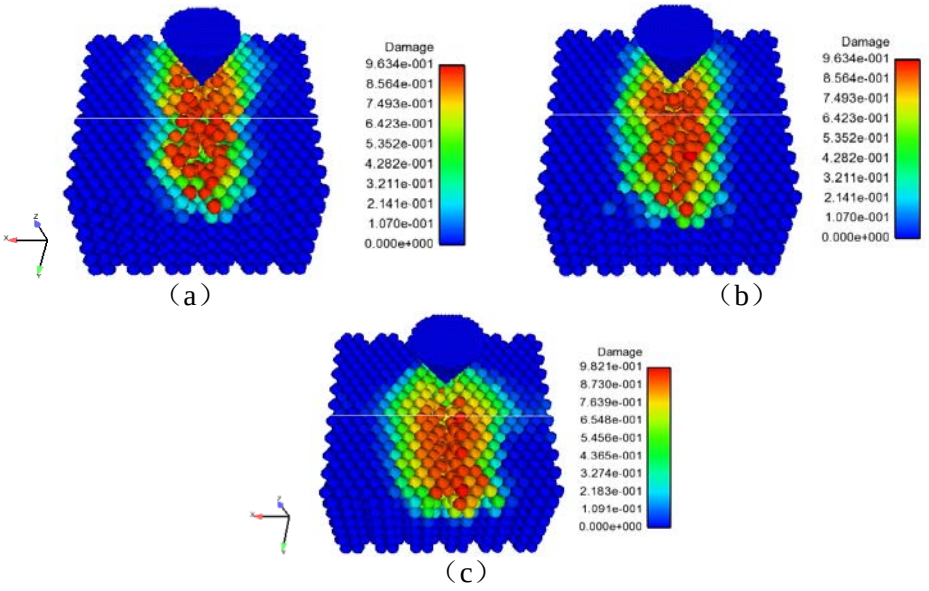

Figure 7. Graph of the damage versus the 70nm scratch distance for the different scratching velocity of （a）$1000nm/s$，（b）$2000nm/s$，（c）$4000nm/s$ respectively.

It can be seen from Figure 7 that when the scratching distance is 70nm and the velocity is $1000nm/s$, $2000nm/s$, $4000nm/s$ respectively, the number and range of severely damaged particles at the interface increases obviously with the increase of velocity.

Considering the influence of different scratching depth on interfacial damage, the scratching speed is set to be $2000nm/s$, respectively, to simulate the cutting process of $5nm$, $10nm$, and $15nm$ depth. The indenter scratches perpendicular to the interface from the end of the sand to the end of the cement paste, where the line is the cement mortar interface. Figure 8 shows the damage range of cement paste and sand at the interface, when the scratching distance is 70nm with different scratching depth.

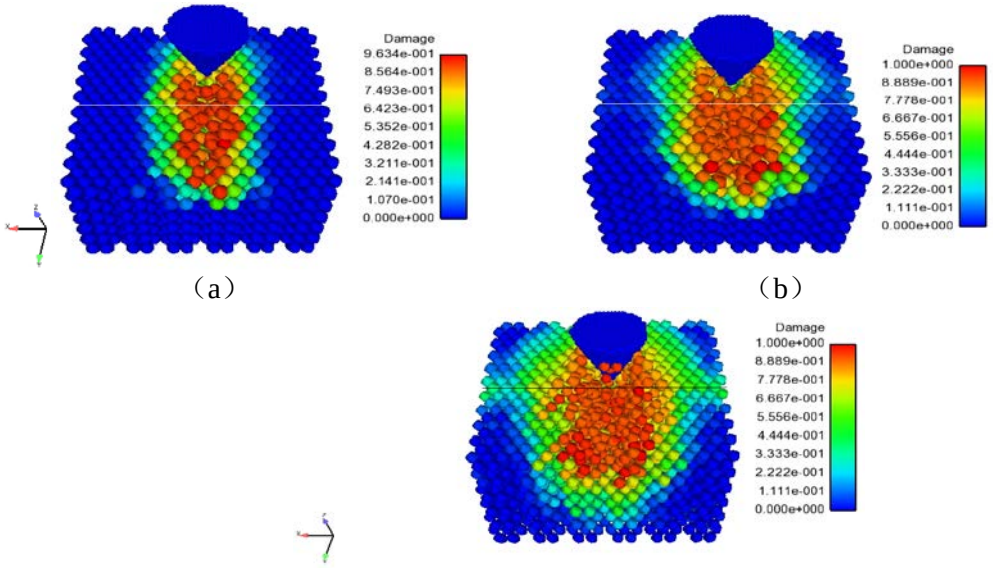

Figure 8. Graph of the damage versus the 70nm scratch distance for the scratching depth 5nm、10nm、15nm respectively.

It can be seen from Figure 8 that when the scratch distance is 70nm, with the depth of scratch increasing, the severely damaged area increases obviously. At the interface, the number and range of damage particles are increasing. When the depth of scratch is 15nm, the damage degree and range are the most serious, and a damage zone has been formed at the interface, which extends to the boundary of the model. In general, with the increase of the scratching depth, the number and range of damage particles of cement paste and sand are increased obviously, and the damage degree is even more serious at the interface.

4. Conclusions

The present paper studied the mechanical properties of ITZ on the nanoscale by simulations for the nanoscratching. Those nanoscratch simulations were performed by moving the indenter along with certain direction either parallel or perpendicular to the interface. The results show the damage evolution, the scratches development and the final damage distributions at the interface during the cutting processes with different cutting speeds and cutting depths. The main conclusions are as follows:

(1) During the process of the indenter scratching parallel to the interface, the cement mortar interface which contacted with the indenter had undergone a complex deformation. Some particles in front of the indenter or on both sides of the indenter were raised and stacked. And a groove was carved. The particles were stacked on both sides of the groove to form a side flow. It can be found that when the speed increased from $1000nm/s$ to $2000nm/s$, the severely damaged area of the cement paste and sand increased obviously. However, when the speed increases from $2000nm/s$ to $4000nm/s$, the damaged area of sand increased gradually. But the damaged area of cement paste had not changed significantly. The main reason for this phenomenon is the cohesive force in the cementitious material. When the scratch depth increased, the severely damaged area increased obviously. Especially when the scratching depth was 15nm, the damage degree and range of cement paste and sand along the interface were basically the same, morphology tended to symmetrical distribution.

(2) During the process which indenter scratching perpendicular to the interface, when the speed increased, the number and range of severely damaged particles at the interface increases obviously. The damage degree and range of cement paste and sand were basically the same, morphology tended to symmetrical distribution. When the depth of scratch increased, the greater the deformation and the severely damaged area increased obviously. When the depth of scratch was 15nm, the damage degree and range were the most serious, and a damage zone had been formed at the interface, which extended to the boundary of the model. In general, with the increase of the depth of scratching, the number and range of damage particles of cement paste and sand are increased obviously, all the results could indicate that the interface between cement and sand is a weak area.

The simulations indicate that the interface between cement and sand is a weak area on the nanoscale.This method for the numerical simulation provides a new direction by studying ITZ. The damage behavior of ITZ on the nanoscale can reflect the macroscopic mechanical properties of cement-based materials. And the simulations can be used to reveal the physical mechanism of deformation and failure of cement-based materials.

Acknowledgements

This research is financially by the National Natural Science Foundation of China (Grant No., 11672101, 11372099, and 51108002). The snapshots were performed using the visualisation tool Ensight.

References

[1] Bentur A, Alexander M. G. A review of the work of the RILEM TC 159-ETC: Engineering of the interfacial transition zone in cementitious composites[J]. Materials and Structures. 2000, 33(2):

82-87.
[2] Nilsen A U, Monteiro P. J. M. Concrete: a three phase material[J]. Cement and Concrete Research. 1993, 23(1): 147-151.
[3] Akçaoğlu T, Tokyay M, Çelik T. Effect of coarse aggregate size and matrix quality on ITZ and failure behavior of concrete under uniaxial compression[J]. Cement and Concrete Composites. 2004, 26(6): 633-638.
[4] Akçaoğlu T, Tokyay M, Çelik T. Assessing the ITZ microcracking via scanning electron microscope and its effect on the failure behavior of concrete[J]. Cement and Concrete Research. 2005, 35(2): 358-363.
[5] Diamond S, Huang J. The ITZ in concrete–a different view based on image analysis and SEM observations[J]. Cement and Concrete Composites. 2001, 23(2): 179-188.
[6] Hu J, Stroeven P. Properties of the interfacial transition zone in model concrete[J]. Interface Science. 2004, 12(4): 389-397.
[7] Wu W. Multiscale modeling and simulation of concrete and its constituent materials: From nano to continuum[M]. ProQuest, 2008.
[8] Hansen T C. Physical structure of hardened cement paste. A classical approach[J]. Materials and Structures, 1986, 19(6): 423-436.
[9] Jennings H. M. A model for the microstructure of calcium silicate hydrate in cement paste[J]. Cement and Concrete Research. 2000, 30(1): 101-116.
[10] Jennings H M. Refinements to colloid model of CSH in cement: CM-II[J]. Cement and Concrete Research, 2008, 38(3): 275-289.
[11] Tennis P D, Jennings H M. A model for two types of calcium silicate hydrate in the microstructure of Portland cement pastes[J]. Cement and Concrete Research, 2000, 30(6): 855-863.
[12] Silling S A, Bobaru F. Peridynamic modeling of membranes and fibers[J]. International Journal of Non-Linear Mechanics, 2005, 40(2):395–409.
[13] Silling S A, Askari E. A meshfree method based on the peridynamic model of solid mechanics[J]. Computers & Structures, 2005, 83(s 17–18):1526-1535.
[14] Zhao Jingjing, Zhang Qing, Huang Dan, Shen Feng. A Peridynamic Approach For The Simulation Of Calcium Silicate Hydrate Nanoindentation[J]. Advances in cement research，2016,28(2): 84-91
[15] Plassard C, Lesniewska E, Pochard I, et al. Investigation of the surface structure and elastic properties of calcium silicate hydrates at the nanoscale.[J]. Ultramicroscopy, 2004, 100(3-4):331–338.
[16] Lesko S, Lesniewska E, Nonat A, et al. Investigation by atomic force microscopy of forces at the origin of cement cohesion.[J]. Ultramicroscopy, 2001, 86(1-2):11–21.
[17] Hamaker H C. The London-van der Waals attraction between spherical particles[J]. Physica, 1937, 4(37):1058-1072.
[18] Bergström L. Hamaker constants of inorganic materials[J]. Advances in Colloid and Interface Science. 1997, 70: 125-169.
[19] Huang D, Lu G, Qiao P. An improved peridynamic approach for quasi-static elastic deformation and brittle fracture analysis[J]. International Journal of Mechanical Sciences, 2015, 94: 111-122.
[20] Allen A J, Thomas J J, Jennings H. M. Composition and density of nanoscale calcium–silicate–hydrate in cement[J]. Nature materials. 2007, 6(4): 311-316.
[21] Fonseca P C, Jennings H M, Andrade J E. A nanoscale numerical model of calcium silicate hydrate[J]. Mechanics of Materials, 2011, 43(8):408–419.
[22] Swope W C, Anderson H C, Berens P. H. A computer simulation method for the calculation of equilibrium constant s for the formation of physical clusters of molecules : application to small water clusters[J]. Journal of Chem Phy. 1982, 76: 637.